Available online at www.sciencedirect.com
ScienceDirect
J. Vis. Commun. Image R. 18 (2007) 68–80
JOURNAL OF VISUAL Communication & IMAGE Representation
www.elsevier.com/locate/jvci

Scale multiplication in odd Gabor transform domain for edge detection

Zhenfeng Zhu [a,b,*], Hanqing Lu [b], Yao Zhao [a]

[a] Institute of Information Sciences, Beijing Jiaotong University, Beijing 100044, China
[b] National Laboratory of Pattern Recognition, Institute of Automation, Chinese Academy of Sciences, Beijing, China

Received 15 February 2006; accepted 7 October 2006
Available online 5 December 2006

Abstract

In this paper, we propose an adaptive edge detection technique based on scale multiplication in odd Gabor transform domain (ESMG). With adjacent scale multiplication in odd Gabor transform domain, a sharpened edge response output is obtained, which can more effectively resist the inverse influence from noise contamination on the performance of edge detector. Based on odd Gabor filter with single scale, it is shown that Rayleigh distribution can be feasibly adopted to model the real pdf of edge response. Thus the pdf of sharpened edge response output can be approximately modeled by an exponential distribution since there exists strong correlation between two edge response outputs with two adjacent scale factors. In determining the threshold for the sharpened edge response, an adaptive strategy is applied, in which the nonlinear relation of the threshold with the mean and variance of exponential distribution is exploited. Moreover, an optimization problem is finally formulated to find the adaptive adjustment factor. The experimental results on both synthetic and real world natural images show that our scheme is robust and takes on good edge detection performance.

Keywords: Edge detection; Gabor transform; Adaptive threshold; Scale multiplication

1. Introduction

Edge detection, which has attracted the attentions of many researchers, is one of the most important areas in lower level computer vision because the success of higher level processing such as object detection, object recognition, and scene interpretation relies heavily on good edge detection. Generally, edges are referred to those pixels around which there is a large gray variation. Most existing edge detection methods are gradient-based, such as some simple edge detection operators Roberts and Sobel as well as some sophisticated operators Canny [1] and Susan et al. [2]. An overview of edge detection techniques was given in [3]. Some new developed edge detection algorithms can be found in [4,5]. In this paper, we focus on the multi-scale analysis of odd Gabor transform to develop a new edge detection technique.

Gabor transform, or named by short time Fourier transform (STFT), can obtain the lower limit of joint time-frequency resolution under Heisenberg Uncertainty Principle. Daugman [6] has taken a deeply investigation on it from the view of visual nerve perceptibility and found that the receptive profile of simple cells in mammalian visual systems can be closely fitted by two-dimension Gabor function. Now two-dimension Gabor transform has obtained comprehensive applications in computer vision field such as image segmentation, object recognition, and so on.

Under Canny's three optimal criterions for edge detection, R. mehrotral [7] pointed out that odd Gabor filter has good edge detection performance. In real applications, as suggested in [7] a simple edge operator should be used to estimate the gradient orientation. Thus the estimation error based on the above simple edge operator, which generally is high especially in the noise case, will largely influence the accurate construction of the odd Gabor filter templates. In addition, we cannot implement the convolution between odd Gabor filter and the input image by using FFT since

* Corresponding author.
E-mail addresses: zfzhu@nlpr.ia.ac.cn (Z. Zhu), luhq@nlpr.ia.ac.cn (H. Lu), yzhao@center.njtu.edu.cn (Y. Zhao).

1047-3203/$ - see front matter © 2006 Elsevier Inc. All rights reserved.
doi:10.1016/j.jvcir.2006.10.001

each pixel corresponds to different odd Gabor filter template.

Multi-scale analysis is a popularly adopted technique in computer vision. A systematic analysis for multi -scale space theory has been given by Tony Lindeberg [8]. The applications of multi scale in edge detection can be dated back to Marr and Hildreth's work [9]. Based on the framework of Canny [1], some techniques for edge detection based on multi scale wavelet transform have been developed [10–12]. In addition, Park et al. [13] have proposed a region based multi scale edge detection method. Recently Zhang [14] extended the ideas of Xu [15] and Sadler [16] and proposed a scale multiplication based edge detection scheme, in which adjacent scales are multiplied in wavelet domain to sharpen the edge responses. In our work, the similar scale multiplication idea was applied to the odd Gabor transform domain, but a more favorable edge response output energy function was presented.

Voorhees et al. [17] pointed that the derivative based edge response can be fitted by Rayleigh distribution, which is also shown in our work to be applicable for odd Gabor filter based edge response. Thus the pdf of sharpened edge response output can be approximately modeled by an exponential distribution since there exist strong correlation between two edge response outputs with two adjacent scale factors. Moreover, an adaptive threshold determining scheme is proposed based on the analysis of the pdf of sharpened edge response output.

This paper is organized as follows: Section 2 gives an introduction to odd Gabor based edge detection and proposes an improvement on it. To sharpen the edge response, a scale multiplication in odd Gabor transform domain is proposed and a more favorable edge response output energy function is given in Section 3. In Section 4, we theoretically analyze the sharpened edge response output energy distribution property and propose an adaptive threshold selection scheme. Some experimental results of synthetic and natural images are presented in Section 5. Finally we give our conclusions in Section 6.

2. Odd Gabor filter based edge detection

Gabor filters, which have been shown to fit well the receptive fields of the majority of simple cell in the primary visual cortex [6], are modulation products of Gaussian and complex sinusoidal signals. A 2D Gabor filter oriented at angle θ is given by:

$$G(x,y,\sigma_g,\omega,\theta) = g(x,y,\sigma_g)\cdot\exp[j\omega(x\cos\theta + y\sin\theta)] \quad (1)$$

where $g(x,y,\sigma_g) = \frac{1}{2\pi\sigma_g^2}\exp[-\frac{1}{2\sigma_g^2}(x^2+y^2)]$ is a Gaussian function, σ_g is the standard deviation of the circle Gaussian along x and y, and ω denotes the spatial frequency.

Fig. 1 shows the even real and odd imaginary parts of a 2D Gabor filter. The Gabor transform on the input image $I(x,y)$ is denoted as:

$$T(x,y) = G(x,y,\sigma_g,\omega,\theta) * I(x,y) \quad (2)$$

where $*$ denotes two-dimensional convolution operator. When $\omega\cdot\sigma \approx 1$ and θ is perpendicular to the edge, i.e. $\theta(x,y) = \partial I(x,y)/\partial y/\partial I(x,y)/\partial x$, the odd Gabor filter $G_o(x,y,\sigma_g,\omega,\theta)$ (the imaginary part of Gabor filter, OGF) has been shown to be an efficient and robust edge detector [7] which offers distinct advantages over traditional edge detectors, such as Roberts, Sobel, etc., and can be comparable even superior to Canny edge detector [1] generally thought as an optimal edge detector.

In filter based edge detection, the filter's smoothing property is crucial for eliminating the inverse influence from noise contaminating. For odd Gabor filter as discussed in [7], it also has such smoothing property and we have the following proposition

Proposition 1. *Let $G_o(x,y,\sigma_g,\omega,\theta)$ to be a 2-D odd Gabor filter and $g(x,y,\sigma_g)$ to be a Gaussian smoothing function with scale σ_g. When $G_o(x,y,\sigma_g,\omega,\theta)$ is convolved with $g(x,y,\sigma_g)$, another odd Gabor filter $G_o(x,y,\sqrt{2}\sigma_g,\omega/2,\theta)$ will be obtained, i.e. we have*

$$c\cdot G_o(x,y,\sqrt{2}\sigma_g,\omega/2,\theta) = G_o(x,y,\sigma_g,\omega,\theta) * g(x,y,\sigma_g)$$

where c is a constant (see Appendix A for detail). One point is that there exists a slight mistake for the proof appeared in [7].

As mentioned in [7], at each pixel some simple edge detectors, e.g. Sobel edge detector, will be utilized to estimate θ that is perpendicular to the edge direction, and then it is used to construct the odd Gabor filter template at that pixel. Thus for an $m\times n$ image $I(x,y)$, it is computationally expensive to construct $m\times n$ odd Gabor filter templates which are applied to convolving with $I(x,y)$. One can build a look-up table of odd Gabor filter templates with the partitioned θ, thus we need only to construct 36 odd Gabor filter templates globally if θ is partitioned by 5°. Even so, we still cannot implement the above convolution by using Fast Fourier Transform (FFT) since each pixel corresponds to different odd Gabor filter template; in other words, all odd Gabor filter templates here are 'local.' In addition, the error influence brought by the estimation of θ will be crucial for constructing odd Gabor filter templates especially in the case of noise contamination. Aiming at the above mentioned problems, here only $\theta_i = \frac{(i-1)\pi}{2}, i = 1,2$ are considered without need to estimate θ at each pixel, thus we have odd Gabor filter at rotation angle θ_i:

$$G_o^i(x,y,\sigma_g,\omega,\theta_i) = g(x,y,\sigma_g)\cdot\sin[j\omega(x\cos\theta_i + y\sin\theta_i)] \quad (3)$$

For a given input image $I(x,y)$, the edge response output energy $E(x,y)$ and the phase angle $A(x,y)$ are defined as

$$E(x,y) = \sqrt{\sum_i [G_o^i(x,y,\sigma,\omega,\theta) * I(x,y)]^2} \quad (4)$$

$$A(x,y) = \arctan\left[\frac{G_o^2(x,y,\sigma_g,\omega,\theta_2) * I(x,y)}{G_o^1(x,y,\sigma_g,\omega,\theta_1) * I(x,y)}\right] \quad (5)$$

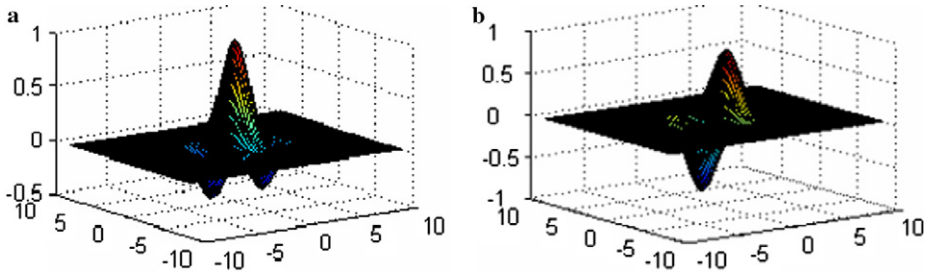

Fig. 1. (a) Even part and (b) odd part of 2D Gabor filter.

Since all G_o^i s can be thought as 'global', thus the convolution between the input image $I(x,y)$ and G_o^i s can be implemented by using FFT.

3. Scale multiplication in odd Gabor transform domain

Multi-scale method is a commonly adopted technique in computer vision. Here, we form the multi-scale odd Gabor filter as

$$G_o^{ik}(x,y,\sigma_g,\omega,\theta_i) = 2^{-2k} G_o^i(2^{-k}x, 2^{-k}y, \sigma_g, \omega, \theta_i) \tag{6}$$

where $k \in Z$ is the scale factor and $i \in [1,2]$ denotes orientation index.

Following the idea of Zhang [14], Xu [15] and Sadler [16], an adjacent scale multiplication in odd Gabor transform domain is performed to obtain a sharpened edge response output $E_s^j(x,y)$, and we have:

$$E_s^j(x,y) = \prod_{k=j}^{j+J} E^k(x,y) \tag{7}$$

$$E^k(x,y) = \sqrt{\sum_i [T_i^k(x,y)]^2} \tag{8}$$

where $E^k(x,y)$ is the edge response in scale k and $T_i^k(x,y) = G_o^{ik}(x,y,\sigma_g,\omega,\theta_i) * I(x,y)$.

As pointed in [14], it is feasible to adopt only two adjacent scales, i.e. $J = 1$, thus we can define the phase angle $A_s(x,y)$ of the sharpened edge response, which will be applied to post-processing for edge response, as

$$A_s^j(x,y) = \arctan\left(\frac{\mathrm{sign}[T_2^j(x,y)] \cdot \left| \prod_{k=j}^{j+J} T_2^k(x,y) \right|}{\mathrm{sign}[T_1^j(x,y)] \cdot \left| \prod_{k=j}^{j+J} T_1^k(x,y) \right|} \right) \tag{9}$$

Note that our definition of $E_s^j(x,y)$ is different from Zhang's [14], which was given as:

$$E_{zs}^j(x,y) = \sqrt{\sum_i} P_i^j(x,y) \tag{10}$$

where $P_i^j(x,y) = \begin{cases} \prod_{k=j}^{j+J} T_i^k(x,y) & P_i^j(x,y) > 0 \\ 0 & \text{else} \end{cases}$. In their case, the summation is conducted over the mutual relative function (scale multiplication across adjacent scales) instead of self-relative function as in Fun. (4). However, the sharpened edge response shown in Fun. (7) can be obtained by directly applying the scale multiplication strategy on the edge response outputs under adjacent scales. Thus compared with the one of $E_{Zs}^j(x,y)$, the output range of edge response can be enlarged greatly by order of square, which will make the following threshold determining for discrimination of edge pixels from non-edge pixels more reliable. Fig. 2 shows the one-dimension sharpened edge response and the output energy with different definitions by Zhang and us. As we can see that more noises with different SNR can be suppressed by our scheme than Zhang's in the case of Gauss white noise added signal, which enables our definition advantage over later since it is more favorable for sharpening edge response. Here, the signal-to-noise ratio (SNR) is defined as $SNR = (S/\sigma_w)^2$, where S denotes the step height of synthetic signal, and σ_w denotes the variance of Gauss white noise added on the noise-free synthetic signal. What we should note is all the outputs in the Fig. 2 are all normalized to 0–1.

4. The adaptive threshold determining for sharpened odd Gabor response

4.1. Rayleigh distribution of edge response based on odd Gabor filter

In [17] Voorhees et al., have pointed that the derivative based edge response can be fitted by Rayleigh distribution. For the first derivative property of odd Gabor filter, the odd Gabor filter based edge response $E(x,y)$ can also be fitted well by Rayleigh distribution. To evaluate the degree of fitness between the real pdf $p(x)$ and the estimated distribution $q(x)$ of odd Gabor based edge response, the Bhattacharya distance is adopted as similarity measure, and we have:

$$s_{p(x),q(x)} = \int_{-\infty}^{+\infty} \sqrt{p(x)q(x)}\mathrm{d}x \tag{11}$$

Let $p_j(x)$, $p_{j+1}(x)$ be the real pdfs of $E^j(x,y)$ and $E^{j+1}(x,y)$ with scale factors j and $j+1$, and $q_j(x)$, $q_{j+1}(x)$ be the corresponding estimated Rayleigh distribution. The Bhattacharya distance based similarities between them are denoted as s_{p_j,q_j} and $s_{p_{j+1},q_{j+1}}$ respectively. Here, $j = 0$ and $\sigma_g = 2.5$ are kept consistent across the proposed scheme.

To verify the assumption of Rayleigh distribution for the odd Gabor based edge response, a sub database of 1000

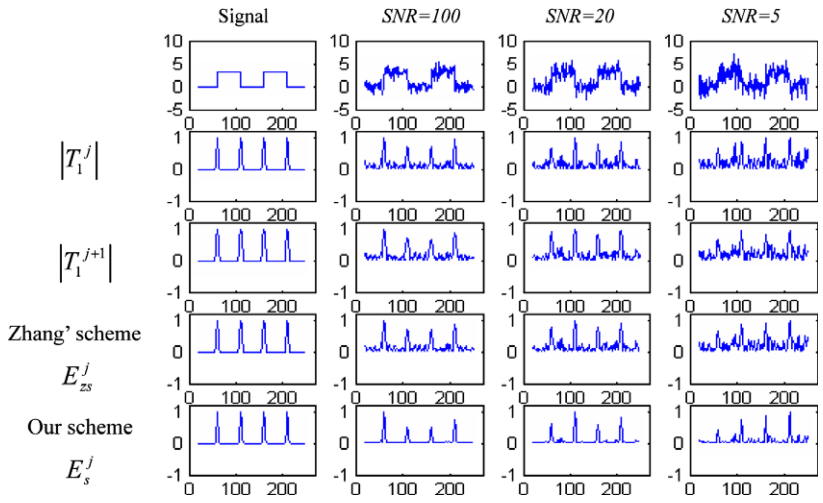

Fig. 2. One-dimension sharpened edge responses and output energy.

images from Corel database with 10 classes and 100 images for each class has been collected. In addition, the cases of images contaminated with Gauss white noise are also considered (only $\sigma_w = 0$ and $\sigma_w = 0.1$ cases are given as in Fig. 3). Fig. 3 shows the histograms of Bhattacharya distance based similarity s between the real pdf and the estimated Rayleigh distribution of odd Gabor filter based edge response. It is obvious to observe for each case that the fitness is good enough between them since most similarity values are over 0.85, which indicates as well that it is feasible to character the real pdf by using the estimated Rayleigh distribution. Thus based on the observed Rayleigh model as in [18], the task of edge detection can be implemented.

4.2. Analysis of the sharpened edge response in odd Gabor transform domain

In edge detection, the strategies of how to determine the threshold to remove those pseudo edge pixels are another extremely important procedure. Before bringing forward an adaptive threshold-determining scheme we first introduce a proposition (see Appendix A for its proof).

Proposition 2. *Given variable X with* $\mathrm{pdf} f_X(x) = \begin{cases} \frac{x}{\sigma_r^2}\exp(-\frac{x^2}{2\sigma_r^2}), & x > 0 \\ 0 & else \end{cases}$ *(i.e. variable X obeys Rayleigh dis-*

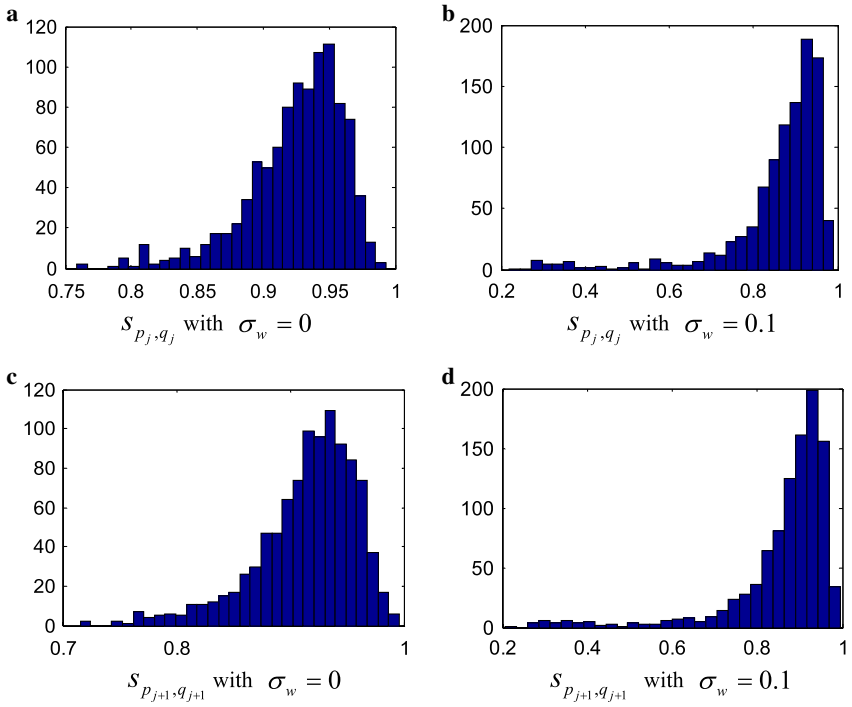

Fig. 3. Histograms of Bhatt. Distance based similarity s between the estimated Rayleigh distribution and the real pdf ($j = 0$).

tribution), then the variable $Y = X^2$ *will obey exponential distribution, i.e. we have* $f_Y(y) = \begin{cases} \frac{1}{\theta}\exp(-\frac{y}{\theta}), & y > 0 \\ 0, & y \leqslant 0 \end{cases}$, where $\theta = 2\sigma_r^2$.

Let μ_e, σ_e be the mean and variance of exponential distribution, then it is easily to obtain $\mu_e = \theta, \sigma_e = \theta$. To estimate the parameter σ_r and θ, a simple median estimation method with low computing expense is adopted and we have

$$\int_0^{\text{median}} \frac{1}{\theta}\exp\left(-\frac{y}{\theta}\right)\mathrm{d}y = \frac{1}{2} \tag{12}$$

Then σ_r and θ can be obtained by

$$\sigma_r = \sqrt{\frac{\text{median}}{2\log(2)}}, \quad \theta = \frac{\text{median}}{\log(2)} \tag{13}$$

For characterizing the sharpened edge response based on the scale multiplication across two adjacent scale factors j and $j+1$ in odd Gabor transform domain, we suppose that there exists strong correlation between edge response outputs $E^j(x,y)$ and $E^{j+1}(x,y)$. To validate it, the Bhattacharya distance is still utilized to character the degree of correlation between them, which are denoted as $s_{p_j,p_{j+1}}$, $s_{q_j,q_{j+1}}$, respectively. Based on the same image database as in Section 4.1, the distribution histograms of $s_{p_j,p_{j+1}}$, $s_{q_j,q_{j+1}}$ are shown in Fig. 4.

Whether the case of the degree of correlation $s_{p_j,p_{j+1}}$ or the case of the degree of correlation $s_{q_j,q_{j+1}}$ is concerned, the assumption of strong correlation between $E^j(x,y)$ and $E^{j+1}(x,y)$ can be ensured, which consequently illuminate that the sharpened edge response E_s^j can be approximately characterized by an exponential distribution according to proposition 2, i.e. we have

$$f_{E_s^j}(e_s^j) = \begin{cases} \frac{1}{\theta}\exp(-\frac{e_s^j}{\theta}), & e_s^j > 0 \\ 0 & \text{else} \end{cases} \tag{14}$$

4.3. An adaptive threshold determining based on exponential distribution

Now we can set a threshold T to distinguish those edge pixels by analysis of the above sharpened edge response output energy distribution $f_{E_s^j}(e_s^j)$. In [17], Voorhees et al. have proposed a threshold selection method based on noise removal probability P, and P can be given as:

$$P = \frac{\int_0^{T_N} f_{E_s^j}(e_s^j)\mathrm{d}e_s^j}{\int_0^{\infty} f_{E_s^j}(e_s^j)\mathrm{d}e_s^j} \tag{15}$$

then we have

$$T_n = -\theta \cdot \log(1-P) \tag{16}$$

Yet such threshold selection comes only from consideration for noise removal and does not take adaptability for edge detection. Based on such threshold selection

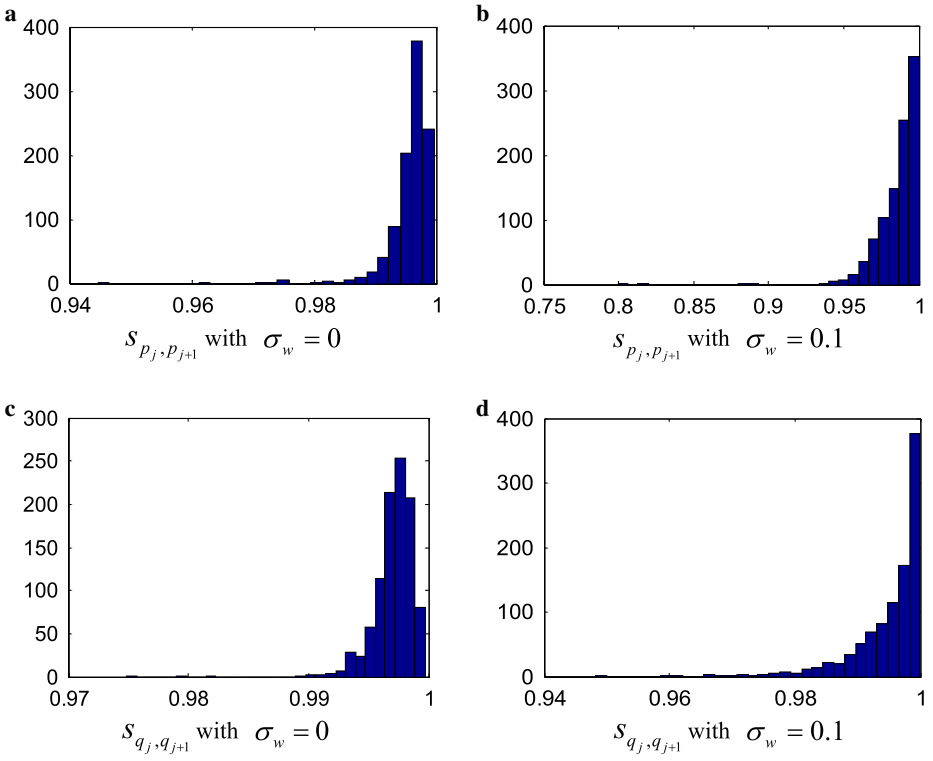

Fig. 4. Histograms of the degree of correlation for the odd Gabor filter based edge responses across two adjacent scale factors ($j = 0$).

strategy, large number of experiments show that lots of details will be lost for large σ_e, and whereas lots of pseudo edges will emerge. In addition, the mean μ_e has not been considered for threshold determining. But based on a large number of experiments and observations, we find that there exist a non- linear relation of threshold with the mean μ_e and variance σ_e of the exponential distribution. The threshold should be decreased correspondingly to have a good visual effect of edge detection when the mean of the distribution is larger. And at the same time, the larger the variance σ_e of the exponential distribution is, the threshold should be increased correspondingly. Generally speaking it is hard to give theoretically such nonlinear relationship. But out of the above observations, an adaptive threshold determining strategy in our edge detection scheme is proposed as

$$T_e = \mu_e + k(\mu_e, \sigma_e)\sigma_e \tag{17}$$

Table 1
The detail information about the synthetic images

Name	Size	No.	*SNR*	Specification
Vertical images	256 * 256	$n_V = 6$	100, 50, 10, 5, 2, 1	The grayscale value is 110 for left part image and 140 for right part
Circle images	256 * 256	$n_C = 6$	100, 50, 10, 5, 2, 1	The grayscale value is 140 for background and 110 for the central circle area

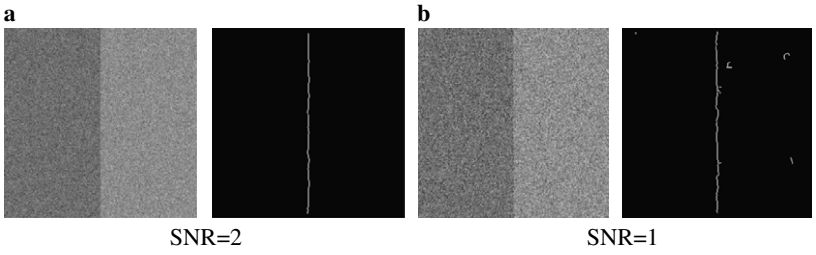

Fig. 5. ESMG based edge detection results for vertical images.

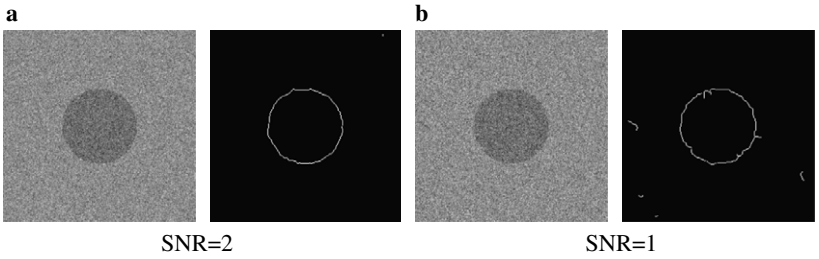

Fig. 6. ESMG based edge detection results for circle images.

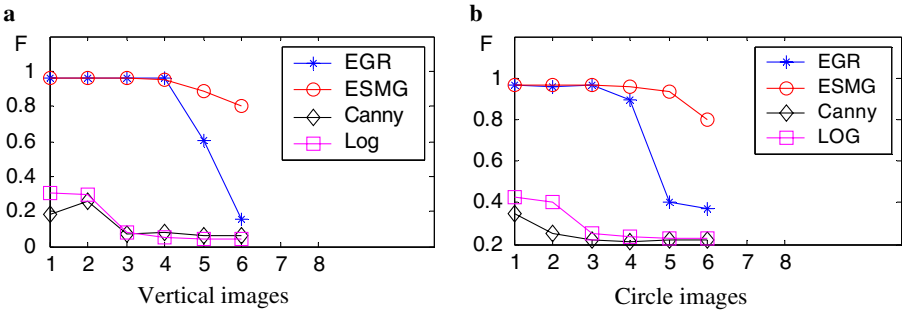

Fig. 7. *F* measure curves for vertical and circle images with different SNR.

where $k(\mu_e,\sigma_e)$ is a nonlinear adaptive adjustment factor with dependence on mean μ_e and variance σ_e, and takes the following expression:

$$k(\mu_e,\sigma_e) = (e_0 - e_1 \cdot \mu_e) \cdot \exp\left(-\frac{\sigma_e}{e_2}\right) \tag{18}$$

where $\{e_i — i = 0,1,2\}$ are some coefficients which will be given in Section 5.

4.4. Post-processing for thresholded edge response

In edge detection, post-processing is another important step. Among gradient-based edge detection operators, Canny's non-max suppression and hysteretic thresholding post-processing method [1] is popularly adopted. In our case, the same post-processing scheme is performed. In addition, the edge connectivity in the final edge map is

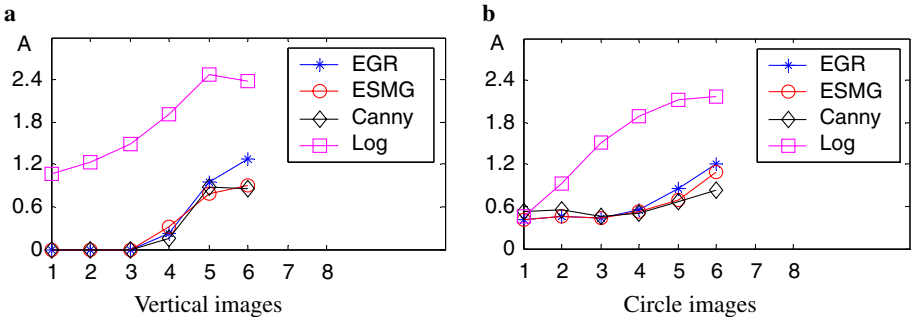

Fig. 8. Localization accuracy A curves for vertical and circle images with different SNR.

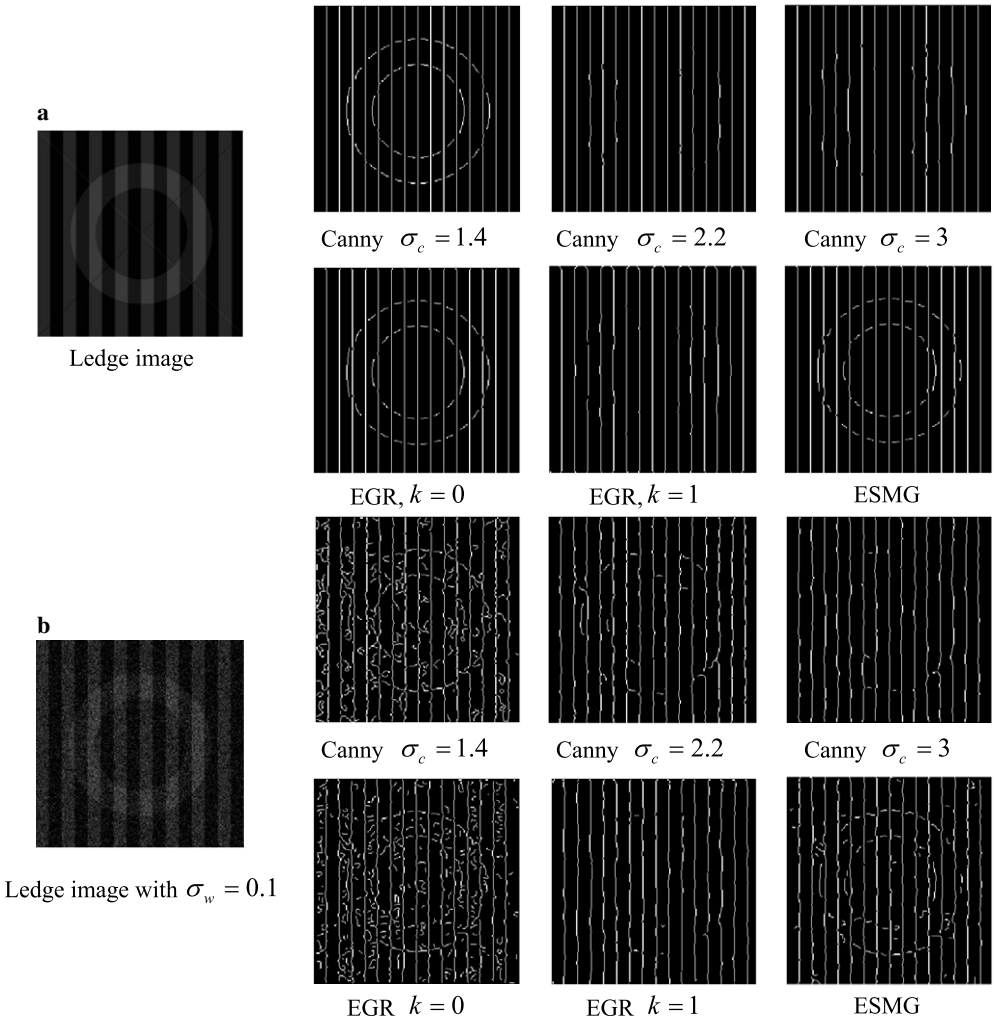

Fig. 9. ESMG based edge detection results for Ledge image.

restrained to no less than three pixels; otherwise, they will be removed as noise.

5. Experimental results and analysis

Because of the subjectivity of edge detection, it is difficult to compare the performance of two edge detectors on most real-world natural images [19]. Here, we use some synthetic [20] and real world images to test the effectiveness of ESMG.

5.1. Synthetic images

In our experiment, two groups of synthetic images, vertical and circle images were tested. The detailed information about the synthetic images is given in Table 1. To evaluate the detection property of ESMG on synthetic images, the measure F (Figure of Merit)[21] and the localization accuracy A [14] are adopted:

$$F = \frac{1}{\max(N_I, N_A)} \sum_{k=1}^{N_A} \frac{1}{1 + \alpha d^2(k)} \tag{19}$$

$$A = \sqrt{\frac{1}{N} \sum_{i=1}^{N} d^2(i)} \tag{20}$$

where N_I is the number of the actual edges and N_A is the number of detected edges, $d(k)$ denotes the distance from the kth detected edge pixel to the corresponding ground truth, α is a scaling constant set to be 1/9 in Pratt's work. N is the number of detected edges with $d(k) \leqslant 4$.We can find from Fun. (19) that the measure F reflects the visual effect of detected edges. The greater the F, the better the detection results. At the same time the measure A shows the location accuracy. The smaller the A, the better the location accuracy will be obtained. For space consideration only the detection results of two synthetic images for each group are shown. From Figs. 5 and 6 we can find that the edge detection results are satisfactory even in the case of $SNR = 1$.

In order to obtain the coefficients $\{e_i — i = 0,1,2\}$ proposed in Fun.(18), the average ratio of the localization accuracy A to the figure of merit F among all the synthetic images is taken as the object function, and thus to obtain the values of all e_is can be formulated into an optimization problem as:

$$\{e_i^{opt} | i = 0,1,2\} = \min_{e_i} \left\{ \frac{1}{n_V + n_C} \sum_{j=1}^{n_V+n_C} \frac{A^j(e_i, i = 0,1,2)}{F^j(e_i, i = 0,1,2)} \right\} \tag{21}$$

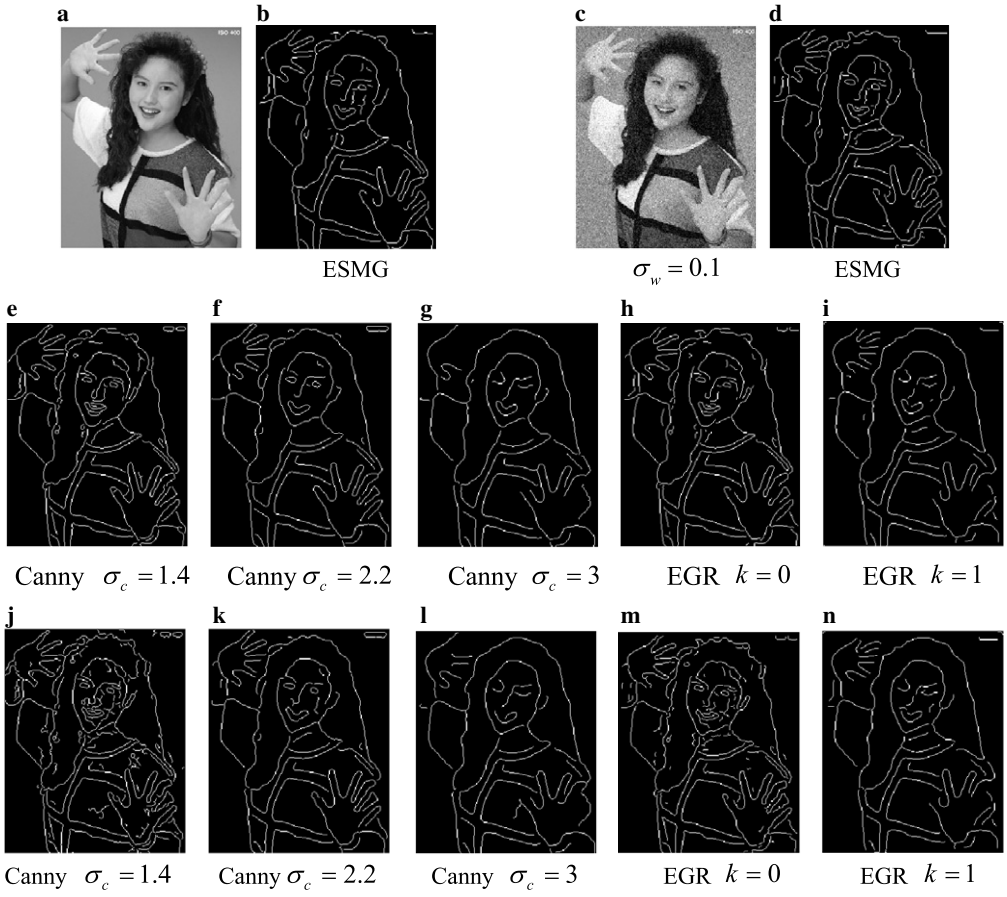

Fig. 10. Edge detection results of 'Woman' image: (a) and (b) original image and edge map based on ESMG, (c) and (d) Gauss white noise added image ($\sigma_w = 0.1$) and edge maps based on ESMG, (e)–(i) edge maps based on Canny and EGR operators with different scales for (a), (j)–(n) edge maps based on Canny and EGR operators with different scales for (c).

where n_V and n_C denote the number of vertical and circle synthetic images, respectively. Generally speaking, it is difficult to find the optimal solution of Fun. (21), thus in this paper the greedy strategy is applied to obtaining the sub-optimal solution as $e_0 = 13.5$, $e_1 = -400$, $e_2 = 0.004$.

Based on the measure F and A we tested four edge detection operators ESMG, Canny, LOG and EGR [18] on the above two groups of synthetic images. As shown in Figs. 7 and 8, the figure of merit measure F based on ESMG keeps stable with variation of SNR, i.e. ESMG is more insensitive to noise. But as far as the location accuracy A is concerned, the LOG operator has the worst location accuracy, and the ESMG, Canny and EGR have similar location accuracy. To consider both measure F and measure A, we can say that ESMG takes on the best edge detection property. Note that the Canny and Log algorithms mentioned above were adopted from image toolbox of Matlab 6.5. The scale σ_c for Canny operator is 2.0 and $\sigma_g = 2.0$ for LOG operator and other parameters are assigned by default.

We also test the ESMG, EGR, Canny edge detection operators on another synthetic image 'ledge' [22], which contains a vertical square wave grating, a ring and two thin diagonal lines. No matter in the case of the original image or the one with Gauss white noise contaminated, the ESMG operator can achieve good visual effects. In addition, the circle edges are all missed for both EGR and Canny operators with the increase of smoothing scale. However, it is also clear that the small smoothing scale is highly sensitive to the noise Fig. 9.

5.2. Natural images

Based on ESMG, Canny and EGR edge operator, Figs. 10–14 show the edge detection results for some real world natural images. For both single scale based Canny and EGR edge operator, with the increase of smoothing scale we can find that more and more local detail information will be filtrated out such as Fig. 10(g) and Fig. 11(g), and the inverse influence brought by noise will be weakened greatly at the same time (see Fig. 12(l), Fig. 13(l) and Fig. 14(l)). Moreover, the difficulty is also explicit for finding a universal optimal smoothing scale, which corresponds to the optimal visual effect of edge detection. That is to say the optimal scale for some images may not be optimal for other images. Of course, the visual effect of edge detection will depend on the viewer's evaluation criterion ultimately.

For the real world images without being contaminated by noise, the visual effects of edge detection based on

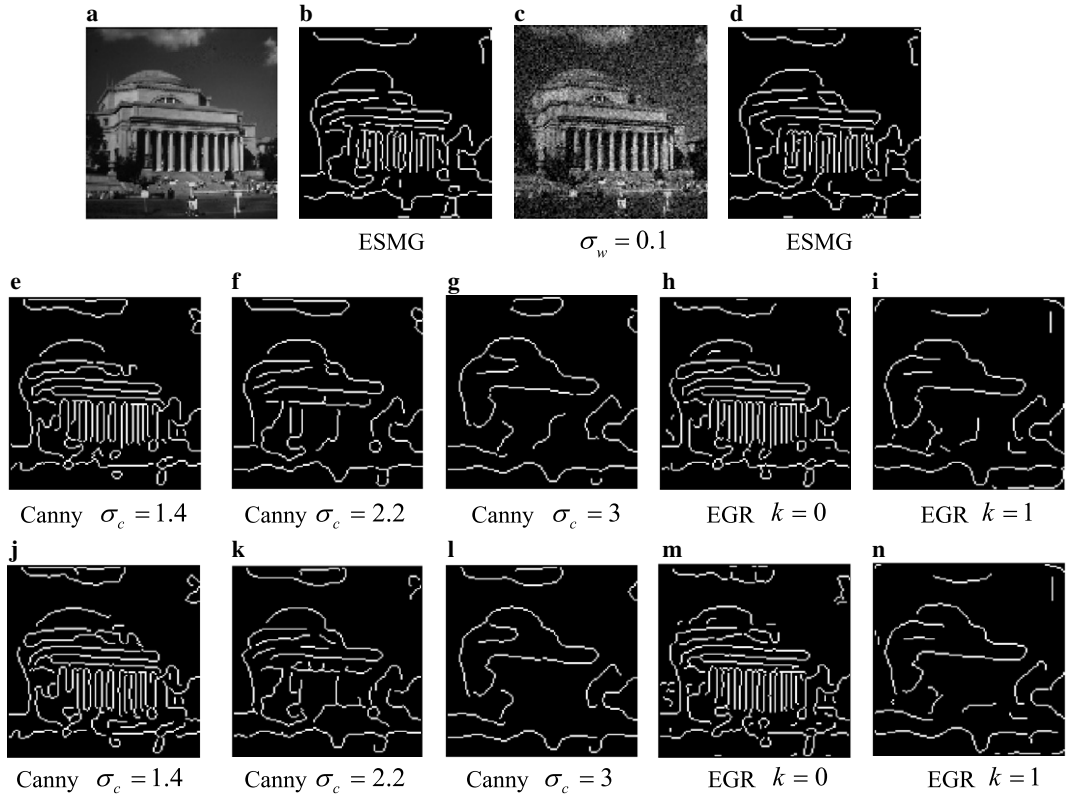

Fig. 11. Edge detection results of 'Building' image: (a) and (b) original image and edge map based on ESMG, (c) and (d) Gauss white noise added image ($\sigma_w = 0.1$) and edge maps based on ESMG, (e)–(i) edge maps based on Canny and EGR operators with different scales for (a), (j)–(n) edge maps based on Canny and EGR operators with different scales for (c).

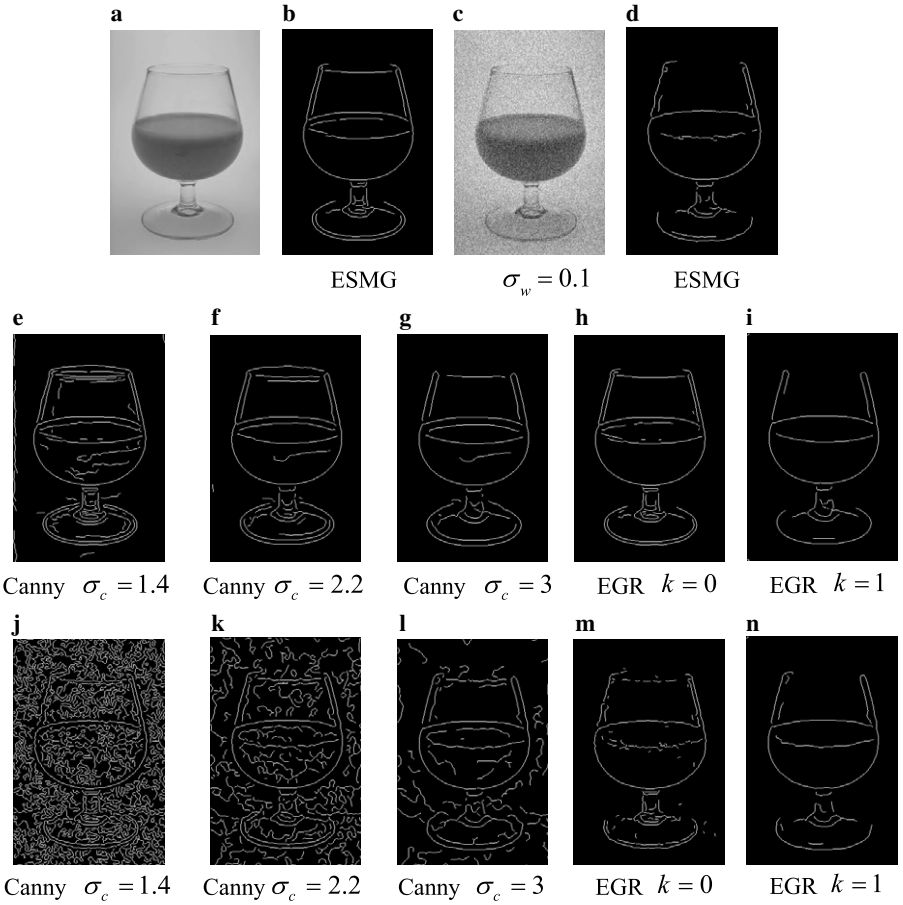

Fig. 12. Edge detection results of 'Cup' image: (a) and (b) original image and edge map based on ESMG, (c) and (d) Gauss white noise added image ($\sigma_w = 0.1$) and edge maps based on ESMG, (e)–(i) edge maps based on Canny and EGR operators with different scales for (a), (j)–(n) edge maps based on Canny and EGR operators with different scales for (c).

ESMG can be comparable to Canny operator with optimal scale (corresponding to optimal visual effect) that is variable for different images, for example, Fig. 10(f) with $\sigma_c = 2.2$ and Fig. 11(e) with $\sigma_c = 1.4$. But as far as noise contaminated images, we can observe that the proposed ESGM is superior to Canny edge operator with the same optimal scale for noise free image as mentioned above. The similar conclusion is also same with EGR operator. One should note that from real application view it is no sense to test all scales to obtain an optimal one for a given image. The robust and good detection performance of the proposed ESMG can contribute to the application of the scale multiplication strategy, which effectively build a bridge between detail keeping and noise resisting.

6. Conclusion

We proposed an adaptive edge detection technique based on the multi scale analysis in odd Gabor transform domain (ESMG). To overcome the shortcomings of original odd Gabor-based edge response obtaining method, an improved scheme is suggested. With adjacent scales multiplication in odd Gabor transform domain, a sharpened edge response output, which can more effectively resist the inverse influence from noise contamination on the performance of edge detector, can be obtained. By analysis of edge response based on odd Gabor filter with single scale, we show that the above sharpened edge response can be approximately characterized by an exponential distribution. Thus as an important step for edge detection, an adaptive threshold-determining scheme was also given, in which the nonlinear relation between threshold and the mean μ_e and variance σ_e of the obtained exponential distribution was explored. In addition, the obtaining of values of coefficients involved in adaptive adjustment factor was formulated into an optimization problem with the average ratio of the localization accuracy A to the figure of merit F among all the synthetic images as object function, and at the same time the greedy strategy was implemented to find the sub-optimal solutions for them. The final experimental results on both the synthetic and real world images show that our edge detection technique is robust and takes on good detection performance.

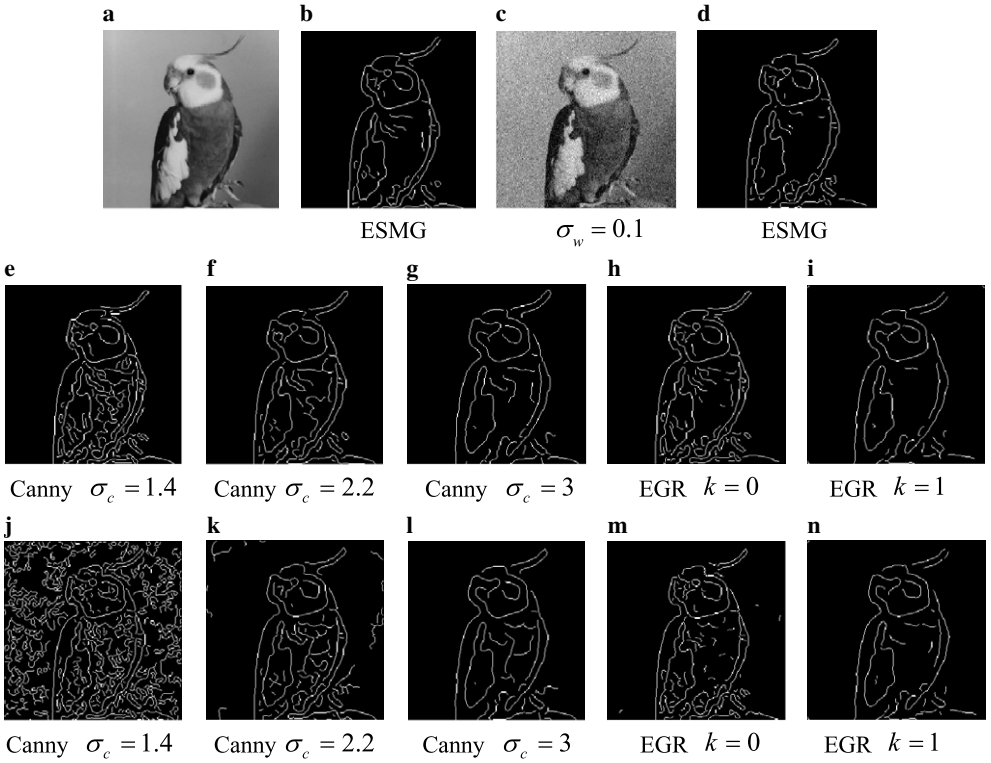

Fig. 13. Edge detection results of 'Bird' image: (a) and (b) original image and edge map based on ESMG, (c) and (d) Gauss white noise added image ($\sigma_w = 0.1$) and edge maps based on ESMG, (e)–(i) edge maps based on Canny and EGR operators with different scales for (a), (j)–(n) edge maps based on Canny and EGR operators with different scales for (c).

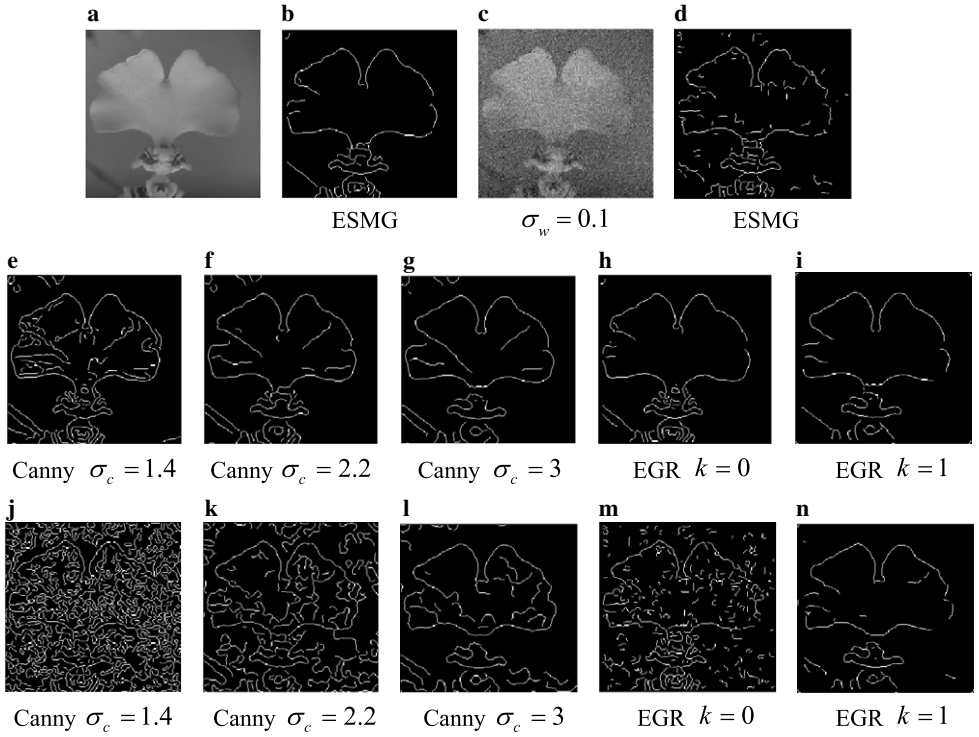

Fig. 14. Edge detection results of 'Flower' image: (a) and (b) original image and edge map based on ESMG, (c) and (d) Gauss white noise added image ($\sigma_w = 0.1$) and edge maps based on ESMG, (e)–(i) edge maps based on Canny and EGR operators with different scales for (a), (j)–(n) edge maps based on Canny and EGR operators with different scales for (c).

Acknowledgments

This work was funded in part by National Natural Science Foundation of China (Nos. 60373028, 60475010 and 90604032), Program for New Century Excellent Talents in University, Specialized Research Fund for the Doctoral Program of Higher Education (No. 20030004016), Specialized Research Foundation of BJTU (No. 2005SZ005), Research Foundation of Beijing Jiaotong University (No. 2005SM013).

Appendix A

Proposition 1. *Let $G_o(x,y,\sigma_g,\omega,\theta)$ to be a 2-D odd Gabor filter and $g(x,y,\sigma_g)$ to be a Gaussian smoothing function with scale σ_g. When $G_O(x,y,\sigma_g,\omega,\theta)$ is convolved with $g(x,y,\sigma_g)$, another odd Gabor filter $G_o(x,y,\sqrt{2}\sigma_g,\omega/2,\theta)$ will be obtained, i.e. we have $c\cdot G_o(x,y,\sqrt{2}\sigma_g,\omega/2,\theta) = G_o(x,y,\sigma_g,\omega,\theta) * g(x,y,\sigma_g)$ where c is a constant.*

Proof. Set $c_1 = \frac{1}{4\pi^2\sigma_g^4}$, then

$$
\begin{aligned}
&G_o(x,y,\sigma_g,\omega,\theta)*g(x,y,\sigma_g)\\
&=\int_{-\infty}^{+\infty}\int_{-\infty}^{+\infty} G_o(x-\lambda,y-\rho,\sigma_g,\omega,\theta)\times g(\lambda,\rho,\sigma_g)\mathrm{d}\lambda\mathrm{d}\rho\\
&=c_1\int_{-\infty}^{+\infty}\int_{-\infty}^{+\infty}\left[\exp(-\frac{x^2-2\lambda x+2\lambda^2+y^2-2\rho y+2\rho^2}{2\sigma_g^2}\right]\\
&\quad\times\sin\{\omega[(x-\lambda)\cos(\theta)+(y-\rho)\sin(\theta)]\}\mathrm{d}\lambda\mathrm{d}\rho\\
&=c_1\int_{-\infty}^{+\infty}\int_{-\infty}^{+\infty}\left[\exp(-\frac{x^2-2\lambda x+2\lambda^2+y^2-2\rho y+2\rho^2}{2\sigma_g^2}\right]\\
&\quad\times\sin\{\frac{\omega}{2}[2(x-\lambda)\cos(\theta)+2(y-\rho)\sin(\theta)]\}\mathrm{d}\lambda\mathrm{d}\rho\\
&=c_1\exp\left(-\frac{x^2+y^2}{4\sigma_g^2}\right)\\
&\quad\times\int_{-\infty}^{+\infty}\int_{-\infty}^{+\infty}\exp\left[-\frac{x^2-4\lambda x+4\lambda^2+y^2-4\rho y+4\rho^2}{4\sigma_g^2}\right]\\
&\quad\times\sin\frac{\omega}{2}[x\cos(\theta)+y\sin(\theta)+(x-2\lambda)\cos(\theta)+(y-2\rho)\sin(\theta)]\mathrm{d}\lambda\mathrm{d}\rho\\
&=c_1\exp(-\frac{x^2+y^2}{4\sigma_g^2})\int_{-\infty}^{+\infty}\int_{-\infty}^{+\infty}\exp\left[-\frac{(x-2\lambda)^2+(y-2\rho)^2}{4\sigma_g^2}\right]\\
&\quad\times\left\{\sin\frac{\omega[x\cos(\theta)+y\sin(\theta)]}{2}\cos\frac{\omega[(x-2\lambda)\cos(\theta)+(y-2\rho)\sin(\theta)]}{2}\right.\\
&\quad\left.+\cos\frac{\omega[x\cos(\theta)+y\sin(\theta)]}{2}\times\sin\frac{\omega[(x-2\lambda)\cos(\theta)+(y-2\rho)\sin(\theta)]}{2}\right\}\mathrm{d}\lambda\mathrm{d}\rho\\
&=c_1\exp\left[-\frac{x^2+y^2}{4\sigma_g^2}\right]\sin\frac{\omega}{2}[x\cos(\theta)+y\sin(\theta)]\\
&\quad\times\int_{-\infty}^{+\infty}\int_{-\infty}^{+\infty}\exp\left[-\frac{(x-2\lambda)^2+(y-2\rho)^2}{4\sigma_g^2}\right]\\
&\quad\times\cos\frac{\omega[(x-2\lambda)\cos(\theta)+(y-2\rho)\sin(\theta)]}{2}\mathrm{d}\lambda\mathrm{d}\rho\\
&\quad+c_1\exp\left[-\frac{x^2+y^2}{4\sigma_g^2}\right]\cos\frac{\omega}{2}[x\cos(\theta)+y\sin(\theta)]\\
&\quad\times\int_{-\infty}^{\infty}\int_{-\infty}^{\infty}\exp\left[-\frac{(x-2\lambda)^2+(y-2\rho)^2}{4\sigma_g^2}\right]\\
&\quad\times\sin\frac{\omega}{2}[(x-2\lambda)\cos(\theta)+(y-2\rho)\sin(\theta)]\mathrm{d}\lambda\mathrm{d}\rho
\end{aligned}
$$

Since the second integration term can be found to be zero, and then

$$
\begin{aligned}
&G_o(x,y,\sigma_g,\omega,\theta)*g(x,y,\sigma_g)\\
&\quad=Ac_1\exp\left[-\frac{x^2+y^2}{4\sigma_g^2}\right]\sin\frac{\omega}{2}[x\cos(\theta)+y\sin(\theta s)]
\end{aligned}
$$

where

$$
\begin{aligned}
A&=\int_{-\infty}^{+\infty}\int_{-\infty}^{+\infty}\exp\left[-\frac{(x-2\lambda)^2+(y-2\rho)^2}{4\sigma_g^2}\right]\\
&\quad\times\cos\frac{\omega[(x-2\lambda)\cos(\theta)+(y-2\rho)\sin(\theta)]}{2}\mathrm{d}\lambda\mathrm{d}\rho\\
&=\sigma_g^2\int_{-\infty}^{+\infty}\int_{-\infty}^{+\infty}\exp\left[-(u^2+v^2)\right]\\
&\quad\times\cos\left\{\omega\sigma_g[u\cos(\theta)+v\sin(\theta)]\right\}\mathrm{d}u\mathrm{d}v\\
&=\sigma_g^2\int_{-\infty}^{+\infty}\int_{-\infty}^{+\infty}\exp\left[-(u^2+v^2)\right]\\
&\quad\times\left\{\cos[\omega\sigma_g\cos(\theta)u]\cos[\omega\sigma_g\sin(\theta)v]\right.\\
&\quad\left.-\sin[\omega\sigma_g\cos(\theta)u]\sin[\omega\sigma_g\sin(\theta)v]\right\}\mathrm{d}u\mathrm{d}v\\
&=\sigma_g^2\left[\int_{-\infty}^{+\infty}\exp(-u^2)\cos(\omega\sigma_g\cos(\theta)u)\mathrm{d}u\right]\\
&\quad\times\left[\int_{-\infty}^{+\infty}\exp(-v^2)\cos(\omega\sigma_g\sin(\theta)v)\mathrm{d}v\right]\\
&=\sigma_g^2\left\{\int_0^{+\infty}\exp\left[-(u-i\frac{\omega\sigma_g\cos(\theta)}{2})^2-\frac{\omega^2\sigma_g^2\cos^2(\theta)}{4}\right]\mathrm{d}u\right.\\
&\quad\left.+\int_0^{+\infty}\exp\left[-(u+i\frac{\omega\sigma_g\cos(\theta)}{2})^2-\frac{\omega^2\sigma_g^2\cos^2(\theta)}{4}\right]\mathrm{d}u\right\}\\
&\quad\times\left\{\int_0^{+\infty}\exp\left[-(v-i\frac{\omega\sigma_g\sin(\theta)}{2})^2-\frac{\omega^2\sigma_g^2\sin^2(\theta)}{4}\right]\mathrm{d}v\right.\\
&\quad\left.+\int_0^{+\infty}\exp\left[-(v+i\frac{\omega\sigma_g\sin(\theta)}{2})^2-\frac{\omega^2\sigma_g^2\sin^2(\theta)}{4}\right]\mathrm{d}v\right\}\\
&=\pi\sigma_g^2\exp(-\omega^2\sigma_g^2\cos^2(\theta)/4)\cdot\exp(-\omega^2\sigma_g^2\sin^2(\theta)/4)\\
&=\pi\sigma_g^2\exp(-\omega^2\sigma_g^2/4)
\end{aligned}
$$

Now set $c = Ac_1$, and we can have $c\cdot G_o(x,y,\sqrt{2}\sigma_g,\omega/2,\theta) = G_o(x,y,\sigma_g,\omega,\theta) * g(x,y,\sigma_g)$

Note: There exists in the original proof of the proposition by Mehrotra [7] a slight mistake for derivation of the value A. In addition, the orientation angleθ of the odd Gabor filter is also considered in our proof.

Proposition 2. *Given variable* X *with pdf* $f_X(x) = \begin{cases} \frac{x}{\sigma_r^2} exp(-\frac{x^2}{2\sigma_r^2}), & x > 0 \\ 0 & else \end{cases}$ *(i.e. variable* X *obeys Rayleigh distribution), then variable* $Y = X^2$ *will obey exponential distribution, i.e.* $f_Y(y) = \begin{cases} \frac{1}{\theta}\exp(-\frac{y}{\theta}), & y > 0 \\ 0, & y \leqslant 0 \end{cases}$. *where* $\theta = 2\sigma_r^2$.

Proof. Let $F_Y(y)$ be the pdf of variable Y, since $Y = X^2 \geqslant 0$, so $F_Y(y) = 0$ for $y \leqslant 0$. For $y > 0$, we have $F_Y(y) = P(Y \leqslant y) = P(-\sqrt{y} \leqslant X \leqslant \sqrt{y}) = \int_{-\sqrt{y}}^{\sqrt{y}} f_X(x)dx$, moreover the pdf $f_Y(y)$ of variable Y can be obtained as:

$$f_Y(y) = \begin{cases} \frac{1}{2\sqrt{y}}[f_X(\sqrt{y}) - f_X(-\sqrt{y})] \\ 0 \end{cases} = \begin{cases} \frac{1}{\theta}\exp(-\frac{y}{\theta}), & y > 0 \\ 0 & \text{else} \end{cases}$$

where $\theta = 2\sigma_g^2$. Thus we can say variable Y takes exponential distribution.

References

[1] J.F. Canny, A computational approach to edge detection, IEEE. Trans. Pattern Anal. Mach. Intell. 8 (6) (1986) 679–698.

[2] S.M. Smith, J.M. Brady, SUSAN—A new approach to low level image processing, Int. J. Comput. Vis. 23 (1) (1997) 45–78.

[3] D. Ziou, S. Tabbone, Edge detection techniques-an overview, Int. J. Pattern Recognit. Image Anal. 8 (4) (1998) 537–559.

[4] P. Meer, B. Georgescu, Edge detection with embedded confidence, IEEE Trans. PAMI 23 (12) (2001) 1351–1365.

[5] S. Ando, Image field categorization and edge/corner detection from gradient covariance, IEEE Trans. PAMI 22 (2) (2000) 179–190.

[6] J.G. Daugman, Complete discrete 2-D Gabor transforms by neural networks for image analysis and compression, IEEE Trans. Acoust. Speech Signal Process. 36 (7) (1988) 1169–1179.

[7] R. Mehrotra, K.R. Namuduri, N. Ranganathan, Odd Gabor filter-based edge detection, Pattern Recognit. 25 (12) (1992) 1479–1494.

[8] T. Lindeberg, Scale-space theory: a basic tool for analysing structures at different scales, J. Appl. Stat. 21 (2) (1994) 224–270.

[9] D. Marr, E. Hildreth, Theory of edge detection, Proc. R. Soc. Lond. B207 (1980) 187–217.

[10] S. Mallat, S. Zhong, Characterizationof signals from multi-scale edges, IEEE Trans. PAMI 14 (7) (1992) 710–732.

[11] M.A. Brown, K.T. Blackwell, H.G. Khalak, et al., Multiscale edge detection and feature binding: an integrated approach, Pattern Recognit. 31 (10) (1998) 1479–1490.

[12] D. Ziou, S. Tabbone, A multi-scale edge detector, Pattern Recognit. 26 (9) pp. 1305–1314.

[13] D.J. Park, K.M. Nam, R.H. Park, Multiresolution edge-detection techniques, Pattern Recognit. 28 (2) (1995) 211–229.

[14] L. Zhang, P. Bao, Edge detection by scale multiplication in wavelet domain, Pattern Recognit. Lett. 23 (14) (2002) 1771–1784.

[15] Y. Xu, J.B. Weaver, et al., Wavelet transform domain filters: a spatially selective noise filtration technique, IEEE Trans. Image Process. 3 (6) (1994) 747–758.

[16] B.M. Sadler, A. Swami, Analysis of multiscale products for step detection and estimation, IEEE Trans. Inform. Theory 45 (3) (1999) 1043–1051.

[17] H. Voorhees, T. Poggio, Detecting textons and texture boundaries in natural images, in: Proc. ICCV (1987) pp. 250–258.

[18] Zhenfeng Zhu, Hanqing Lu, Edge detection based on odd Gabor filter and Rayleigh distribution, J. Image Graph. China 10 (7) (2005) 821–827.

[19] M. Heath, S. Sarkar, T. Sanocki, K. Bowyer, Comparison of edge detector: a methodology and initial study, Comput. Vis. Image Understand. 69 (1) (1998) 38–54.

[20] W. Zhou, A new method of edge detection [EB/OL], <http://prettyview.com/edge/nsedge.shtml#to>.

[21] I.E. Abdou, W.K. Pratt, Quantitative design and evaluation of enhancement/ thresholding edge detectors, Proc. IEEE 67 (5) (1979) 753–763.

[22] <http://w3.ualg.pt/~dubuf/pubdat/ledge/>.